



Numerical study of turbulent flow in USBR VI stilling basin

Ehsan Behnamtalab¹ · Vahidreza Maskani¹ · Hamed Sarkardeh¹

Received: 18 January 2023 / Accepted: 23 May 2023 / Published online: 9 June 2023
© The Author(s) 2023

Abstract

The USBR VI stilling basin is one of the oldest basins designed to dissipate the energy at the outlet of pipes. In this study, the effect of two parameters including the Froude number (Fr) of inlet flow to the basin and the ratio of basin width to equivalent depth of the inlet flow (W/D) on the characteristics of mean and turbulent flow inside the USBR VI stilling basin were investigated, numerically. Reynolds Averaged Navier–Stokes (RANS) equations were solved with Re-Normalization Group (RNG) k - ϵ turbulence model. Results showed that by increasing W/D , from 3.50 to 9.23, decreasing rate of the average velocity at the end of the basin to the average velocity of the inflow increases from 80 to 97% and decreasing rate of the maximum velocity at the end of the basin to the average velocity of the inflow increases from 40 to 87%. Also, by increasing W/D , from 3.50 to 9.23, the average turbulent dissipation rate in the whole basin increases to 4.5 times, moderately. Moreover, by increasing W/D , from 3.50 to 9.23, the dissipation of turbulent flow energy in the basin becomes four times. Therefore, to design a USBR VI stilling basin based on the existing conditions, W/D recommended to increase as much as possible until nearly 10.

Keywords USBR VI stilling basin · Turbulent dissipation · Turbulent kinetic energy · Numerical model · RANS

List of symbols

A	Cross-sectional area of incoming flow
a	Baffle distance from inlet
b	Baffle height
D	Depth of incoming flow
d	Endsill height
D_o	Inlet pipe diameter
Fr	Froude number of incoming flow
g	Gravity acceleration
H	Basin wall height
k	Turbulent kinetic energy
L	Basin length
P	Pressure
Q	Inlet flow rate
t	Baffle thickness
u	Velocity in x -direction
\bar{u}	Mean velocity of incoming flow

u_{Max}	Maximum velocity
W	Basin Width
x^*	Normalized x -Position ($x^* = x/L$)
y^*	Normalized y -Position ($y^* = y/W$)
z^*	Normalized z -Position ($z^* = z/H$)

Greek Symbols

ϵ	Turbulent dissipation rate
μ	Dynamic viscosity
ρ	Water density

Introduction

The kinetic energy dissipated at the end of spillway has been one of the most important issues for researchers in the recent years. The flow downstream of the spillway structure should return to the normal state before entering the river (Pagliara and Palermo 2012). The kinetic energy dissipation at the end of the spillway is done by various structures as well as stilling basins. The dissipative process that occurs in the stilling basin is a major topic in river engineering. The energy dissipation has to be correctly evaluated to prevent structural stability risks and to optimize the hydraulic performance of the energy dissipator itself (Shahheydari et al. 2015). Among the types of stilling basin, there are basins where the kinetic energy dissipation is done by the collision of a flow with

✉ Ehsan Behnamtalab
e.behnamtalab@hsu.ac.ir

Vahidreza Maskani
vrm1376@gmail.com

Hamed Sarkardeh
sarkardeh@hsu.ac.ir

¹ Department of Civil Engineering, Hakim Sabzevari University, Sabzevar, Iran

an obstacle. Baffle placement is widely used in hydraulic structures to dissipate kinetic energy in low-head outlets and spillways (Bestawy et al. 2013; Vischer 2018).

In the impact stilling basins, the water flow impact to the various baffles along the path and prevents it from accelerating or energy dissipated inside the stilling basin by installing baffles with different geometries inside it (Goel 2008). One of the most common types of these basins is the USBR VI stilling basin. The USBR VI stilling basin is one of the oldest basins designed to dissipate energy from the outlet of pipes or culverts.

According to the USBR report, Fr of the inlet flow to this basin considered between 1 and 10. This basin is used in most irrigation and drainage projects and also surface water collection network where Fr of inlet flow is low (Beichley 1971). In this basin, there is a baffle in the middle and an end sill at the end. The middle baffle has two parts, vertical and horizontal. The vertical part is located in front of the inlet flow and has a certain distance from the bottom of the basin so the inlet flow can move downstream from below. Horizontal part turns part of the input flow upwards to dissipate more energy from the input flow. Most of the energy of the incoming flow to the basin dissipated by impact to the baffle and the turbulence created upstream of the baffle. In order to hydraulically design of this basin, a relation between Fr and WD is presented. To calculate the Fr of the incoming flow, it must first determine the equivalent depth of the input flow according to Beichley (1971):

$$D = \sqrt{A} = \sqrt{Q/\bar{u}} \quad (1)$$

where A is the cross section of the inflow to the basin, Q is the volume flow rate to the basin and \bar{u} is the average velocity of the inflow. Therefore, Fr of the incoming flow is (Beichley 1971):

$$Fr = \frac{\bar{u}}{\sqrt{g \times D}} \quad (2)$$

By Fr and D , the width of the basin can be calculated with using Eq. 3. The full dimensions of the USBR VI stilling basin depend on its width, and by calculating the width of the basin, the dimension of the other parts is Brevard (1971):

$$\frac{W}{D} = 2.86 \times Fr^{0.575} \quad (3)$$

Dissipation of energy in this basin is carried out by flow striking the baffle and being turned upstream by the horizontal part of the baffle and by the floor, in vertical eddies. Comparing the energy loss in this basin with the losses in a hydraulic jump stilling basin shows that the USBR VI stilling basin is more efficient (Hager 2013).

A small notch or drain is usually included in the end sill to facilitate basin drainage during periods of low or no flow (Tullis and Bradshaw 2015). Since most of the energy dissipation occurs before the flow passes below the baffle, very little downstream stilling basin length is usually required. Therefore, the much shorter length compared to the hydraulic jump is one of the important advantages of this type of this basin (Young 1978). Other very useful characteristics of this basin is that it does not need tailwater for satisfactory performance. Of course, the presence of tailwater causes the velocity of the outflow from the basin to decrease and the profile of the outflow water level to become smoother (Beichley 1971). Previous researches show that the increase in the performance of the basin with the presence of tailwater occurs only when the ratio of the depth of the tailwater to the diameter of the inlet pipes greater than 0.65 (Blaisdell 1992). In order to prevent the basin from being completely filled with sediment and also to wash the sediment after a long period of sedimentation inside the basin, two notches should be added to the baffle. These notches wash the sediment by creating concentrated jets (Young 1978).

Several improving on designs have been reviewed and implemented on this basin. Verma and Goel, by using a physical model tried to reduce the scouring downstream the basin. They with changing the geometry of the basin such as an intermediate sill below the baffle and a splitter block aligned with the incoming flow. These changes caused a major reduction in scouring downstream of the basin. They also studied the location of the inlet pipe to the basin using a physical model, which calls into question whether the baffle is effectively utilized (Verma and Goel 2003).

Behnamtalab et al. studied the stilling basin USBR VI using comprehensive research (Behnamtalab et al. 2019, 2017, 2022). In part of their research, they investigated the flow field in the basin using a numerical model. They explained how the flow enters the basin and spreads it behind the baffle, as well as how it passes under the baffle. They explained the changes in average velocity in all directions, volume flow rate distribution across the width and several other characteristics of the flow inside the basin and its downstream. Also, they made various changes in the geometry of the basin in order to modify the flow pattern and reduce scouring downstream of the basin. They suggested that gradually increasing the width of the basin after the baffle significantly reduces scour downstream of the basin. Table 1 has been prepared in order to brief review the previous researches in the field of USBR VI stilling basin.

A review of the previous researches showed that understanding flow pattern inside the basin, familiarity with the mechanism of the energy dissipation and the characteristics of the turbulent flow in different conditions can help the optimal design of the basin. Since numerical simulations

Table 1 Summary of literature review especially on USBR VI stilling basin and its optimization

Author	Study method	Input parameters	Output
Beichley (1971)	Experimental	<i>W/D</i> and <i>Fr</i>	This basin is more efficient than hydraulic jump Basin design with dimensionless parameters ($1 < Fr < 10$)
Peterka (1978)	Experimental	Volume flow rate	Using several basins where volume flow rate is very high
Rice and Kem (1991)	Experimental	Tailwater	Increasing the performance of the basin
Verma and Goel (2000)	Experimental	Intermediate sill below the baffle and a splitter Behind the Baffle Wall	Reducing the scouring downstream the basin
Khan (2011)	Numerical	height of the wing walls	Energy dissipation inside the basin
Tiwari and Goel (2016)	Experimental	distance between the baffle and the inlet pipe	Reducing the scouring downstream the basin
Tiwari et al. (2022)	Experimental	Splitter Block Shape	Reducing the length of the basin Reducing the scouring downstream the basin
Aleyasin et al. (2015)	Experimental	Splitter Shape behind the Baffle Wall	Velocity field
Behnamtalab et al. (2019, 2017, 2022)	Numerical	<i>W/D</i> and <i>Fr</i>	Qualitative and quantitative flow field Basin geometry optimization Basin optimization by entropy generation index

can be used to extract more details of the flow pattern and turbulent flow characteristics (Baranya et al. 2015; Barati et al. 2018; Fadafan and Kermani 2017). Therefore, in this study, using numerical simulations to study the flow pattern and turbulent flow characteristics of the USBR VI stilling basin are discussed. Considering that the parameter of *Fr* of inlet flow and also *W/D* are among the important and influential parameters on the hydraulic characteristics of the flow inside the basin, the effects of these two parameters on turbulent flow characteristics are investigated, numerically.

Governing equations and numerical simulation

In this study, RANS equations are used to simulate turbulent flow. These equations, which are the equations of time-averaged of motion for fluid flow, are used to describe turbulent flows and incompressible Newtonian fluid (Anderson and Wendt 1995; White 2006; Hirt and Nichols 1981). The continuity and momentum equations are:

$$\frac{\partial u_i}{\partial x_i} = 0 \tag{4}$$

$$\frac{\partial u_i}{\partial t} + u_i \frac{\partial u_j}{\partial x_i} = -\frac{1}{\rho} \frac{\partial p}{\partial x_j} - \frac{\partial(\overline{u_i u_j})}{\partial x_i} \tag{5}$$

where ρ is the density of the fluid, u_i are the time-averaged velocities, and p is the time-averaged pressure. Equations 6 and 7 are also the turbulent kinetic energy or TKE (k) and

the turbulent dissipation rate (ϵ), respectively (Hoffman and Johnson 2007).

$$\frac{\partial k}{\partial t} + u_i \frac{\partial k}{\partial x_i} = \frac{\partial}{\partial x_i} \left(\frac{t}{\sigma_k} \frac{\partial k}{\partial x_i} \right) + t \left(\frac{\partial u_i}{\partial x_j} + \frac{\partial u_j}{\partial x_i} \right) \frac{\partial u_i}{\partial x_j} - \epsilon \tag{6}$$

$$\frac{\partial \epsilon}{\partial t} + u_i \frac{\partial \epsilon}{\partial x_i} = \frac{\partial}{\partial x_i} \left(\frac{t}{\sigma_\epsilon} \frac{\partial \epsilon}{\partial x_i} \right) + C_{\epsilon 1} \frac{\epsilon}{k} t \left(\frac{\partial u_i}{\partial x_j} + \frac{\partial u_j}{\partial x_i} \right) \frac{\partial u_i}{\partial x_j} - C_{\epsilon 2} \frac{\epsilon^2}{k} \tag{7}$$

The turbulent viscosity or eddy viscosity t also calculated:

$$t = C_\mu \frac{k^2}{\epsilon} \tag{8}$$

The coefficients used in the above equations include C_μ , $C_{\epsilon 1}$, $C_{\epsilon 2}$, σ_k and σ_ϵ in the RNG turbulence model are 0.085, 1.063, 1.72, 0.7179 and 0.7179, respectively. In order to accurately simulate the turbulent flow in open channel flows, the best turbulence model should be chosen, so it is very necessary to investigate the effect of different turbulence models on the results of the flow field (Farhadi et al. 2018; Talebpour and Liu 2018; Jafari-Nodoushan et al. 2016; Tajnesaie et al. 2018). The choice of the RNG $k - \epsilon$ turbulence model is due to the fact that it has given very good results in several studies of simulation of turbulent flows and is also very simple (Rodriguez et al. 2004; Rady 2011; Usta 2014; Zachoval and Roušar 2015; Babaali et al. 2015; Amorim et al. 2015; Ghazizadeh and Moghaddam 2016). Also, in this study, the results of flow field simulation in basin have been compared with RNG $k - \epsilon$ turbulence models, $k - \epsilon$ and $k - \omega$ and the results showed that

the RNG $k - \epsilon$ turbulence model predict turbulent flow in the USBR VI stilling basin with higher accuracy.

In Fig. 1, the flowchart of the research method is presented for the numerical simulation of the USBR VI stilling basin and investigation of the turbulent flow field in it.

In this study, Flow3D software (Science 2008) is used to simulate the USBR VI stilling basin. The Finite Volume Method (FVM) is employed to solve three-dimensional (3D) flow equations. Fractional Area–Volume Obstacle Representation (FAVOR) method (Hirt and Sicilian 1985) is also selected to detect the geometry of the structure. The FAVOR method uses the value of cell porosity and determines its value with a number between 0 and 1, and with this value, the geometry of the structure and the flow of fluid will be separated from each other. This model also uses FVM and VOF method to discretize and solve the governing equations and tracking free surface of water. In VOF method (Hirt and Nichols 1981), a quantity is defined in each cell that indicates the ratio of cell water filling. A value of one indicates that the cell is completely filled with water and a value of zero indicates that there is no fluid inside the cell. By knowing this quantity, the location of the water surface and its angle between the cells of the solution field can be detected by the model. In addition, in simulating the USBR VI stilling basin, No-Slip conditions are used at the contact surface of the fluid flow with the wall (Hirt 2011).

The Generalized Minimal Residual (GMRES) method has been used as an implicit pressure–velocity solver to create a pressure–velocity coupling. This method is very accurate and efficient for a wide range of problems and has excellent convergence, symmetry and speed properties. However, it uses more memory than other methods (Hirt 2011). Whenever the velocity, Reynolds stress and continuity equation residuals are less than 10^{-6} , the convergent numerical solution is considered. Also, in all numerical models in this research, water density and dynamic viscosity and its temperature were considered 1000 kg/m^3 , 0.001 kg/m^3 and $20 \text{ }^\circ\text{C}$, respectively.

According to the contents presented in the introduction, two important and influential parameters on the flow field in the USBR VI stilling basin include the Fr of inlet flow and the W/D . For this purpose, 3 basins with different W/D are simulated and 5 different Fr are also evaluated in each basin. Therefore, in order to study the turbulent flow field, 15 different numerical simulations are performed. The general shape of the stilling basin and its characteristics are shown in Fig. 2. The bottom end of the inlet pipe to the basin is considered as the origin of the coordinate system. For this purpose, to determine the position of any point in the stilling basin, dimensionless relations $x^* = x/L$, $y^* = y/W$ and $z^* = z/H$ are used, where x^* , y^* and z^* are no-dimension locations of each point. In the presented relations, x , y and z are the locations of each point

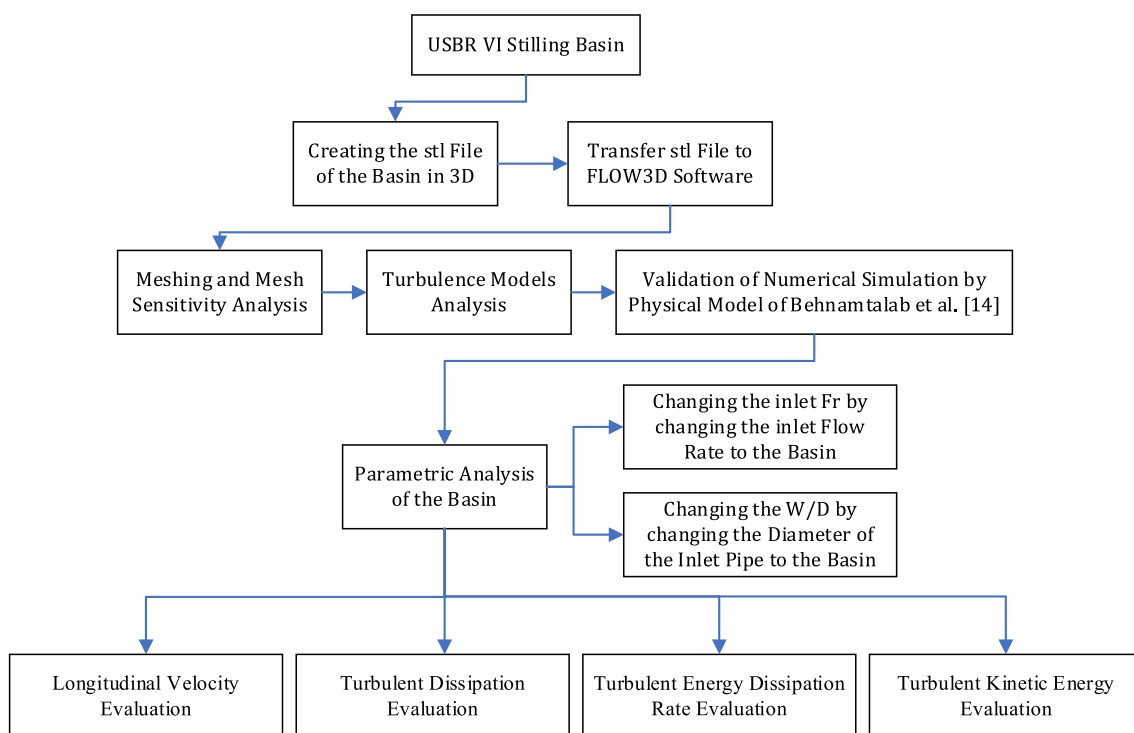


Fig. 1 Flowchart of the research method

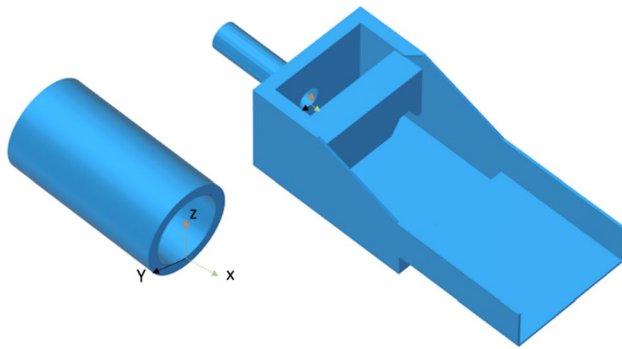


Fig. 2 Geometry of the USBR VI stilling basin and coordinate system origin

in the Cartesian coordinate system and L , W and H are the length, width and height of the stilling basin, respectively.

As mentioned earlier, all dimensions of the USBR VI stilling basin depend on its width. The width of the basin is considered 45 cm in all numerical models. The desired width is in accordance with the physical model of Behnamtalab et al. (2017). Table 2 shows the USBR VI stilling basin characteristics in numerical models.

In this table, W is the basin width, L is the basin length, H is the basin height, d is the endsill height, a is the distance from the beginning of the basin to the vertical baffle, b is the

vertical baffle height and t is the baffle thickness. To create three different W/D , as mentioned, the basin width fixed and the inlet pipe diameter D_o are changed. Therefore, considering the inlet pipe diameter equal to 5.5, 8.5 and 14.5 cm and the basin width equal to 45 cm, according to Table 3, three different W/D equal to 9.23, 5.97 and 3.50 is created.

Using Eq. 3 for three different W/D of 9.23, 5.97 and 3.50, the standard design Fr are 7.67 (Run 3), 3.61 (Run 8) and 1.42 (Run 13), respectively. Therefore, to fully investigate the hydraulic flow characteristics in each W/D , two Fr higher than the standard Fr and two Fr lower than the standard Fr are considered.

The computational domain continued downstream the basin or the channel downstream the basin until a perfectly uniform flow was created. Also, upstream the basin, the inlet pipe length to the basin was considered so that the flow at the end of the pipe or at the entrance to the basin is fully developed. Therefore, based on the relation of the boundary layers in turbulent flow, the inlet pipe length to the basin in models with $W/D = 9.23$ is equal to 2 m, in models with $W/D = 5.97$ equal to 3 m and in models with $W/D = 3.50$ is equal to 5 m. In all models, the tailwater for the best basin performance was 16 cm ($d + b/2$) (Beichley 1971). Figure 3 shows the mesh created on the USBR VI stilling basin. In order to meshing this basin, two different mesh blocks have been used. The inlet pipe to the basin

Table 2 USBR VI stilling basin numerical model characteristics (in cm)

W	L	H	d	b	a	t
45	60	33.8	7.5	16.9	22.5	3.5

Table 3 Characteristics of different numerical models

Model Name	Inlet pipe diameter (cm) D_o	Depth of incoming flow (cm) D	Basin width (cm) W	Froude number Fr	Mean velocity of incoming flow (m/s) \bar{u}	Inlet discharge (L/s) Q	W/D
Run 1	5.5	4.87	45	5.48	3.79	9	9.23
Run 2	5.5	4.87	45	6.70	4.63	11	9.23
Run 3	5.5	4.87	45	7.67	5.30	12.6	9.23
Run 4	5.5	4.87	45	8.52	5.89	14	9.23
Run 5	5.5	4.87	45	9.74	6.73	16	9.23
Run 6	8.5	7.53	45	1.85	1.59	9	5.97
Run 7	8.5	7.53	45	2.67	2.29	13	5.97
Run 8	8.5	7.53	45	3.61	3.10	17.6	5.97
Run 9	8.5	7.53	45	4.51	3.88	22	5.97
Run 10	8.5	7.53	45	5.54	4.76	27	5.97
Run 11	14.5	12.85	45	0.92	1.03	17	3.50
Run 12	14.5	12.85	45	1.19	1.33	22	3.50
Run 13	14.5	12.85	45	1.42	1.60	26.4	3.50
Run 14	14.5	12.85	45	1.73	1.94	32	3.50
Run 15	14.5	12.85	45	2.05	2.30	38	3.50

Fig. 3 Computational grid

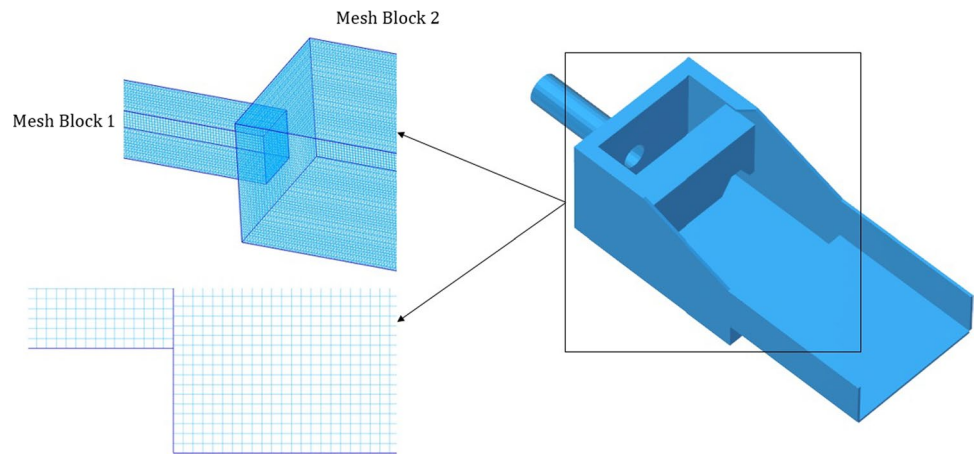


Table 4 Boundary conditions in mesh blocks

	X_{min}	X_{max}	Y_{min}	Y_{max}	Z_{min}	Z_{max}
Mesh block No.1	Volume flow rate	Symmetric	Wall	Wall	Wall	Wall
Mesh block No.2	Symmetric	Outflow	Wall	Wall	Wall	Symmetric

Table 5 Total kinetic energy in the mesh Block 2 for different meshes

	Mesh 1	Mesh 2	Mesh 3	Mesh 4	Mesh 5
Mesh cell size (mm)	6	8	10	12	14
Total turbulent kinetic energy (J)	1.556	2.825	3.501	4.391	4.379

has meshed by Block 1 and the stilling basin and its downstream channel has been meshed by Block 2. The flow in Block 1 enters to the inlet pipe (x_{min}) with a certain volume flow rate with a uniform flow. At the end of Block 2, the flow will be out of the computational domain (x_{max}) using the outlet boundary condition. Symmetry boundary condition was used between the two meshed blocks. Also, to simulate the water surface in contact with air (z_{max}), the symmetry is used to create a relative zero-pressure. All boundary conditions in Blocks 1 and 2 are presented in Table 4.

In order to study the independence of the research results from the mesh size, Run 13 model with five different cell sizes in the range of 6–14 mm is conducted. In all cases, the turbulence kinetic energy in the whole mesh Block 2 was considered as a criterion for selecting the optimal cell size. The effect of cell size on the total turbulence kinetic energy prediction accuracy is shown in Table 5 and Fig. 4.

The results show that the total turbulence kinetic energy for Mesh 1 and Mesh 2 is completely different from the other three meshes, but there is a slight difference between the predicted total turbulence kinetic energy of Mesh 4 and

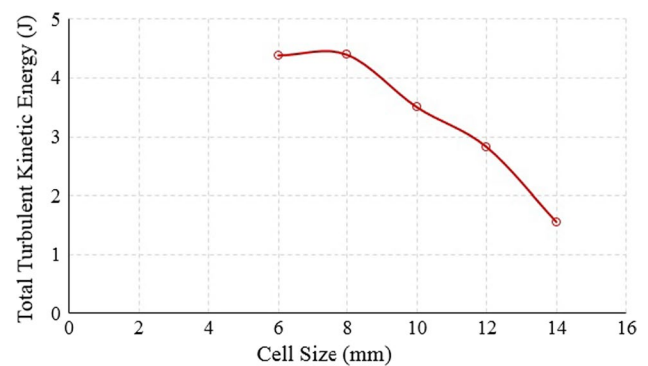


Fig. 4 Variation of the total turbulent kinetic energy for different cell sizes

Mesh 5. Therefore, to reduce the simulation time, Mesh 4 is selected as the optimal mesh.

Results and discussion

In this part, the numerical model will first be validated and then the turbulent flow field inside the stilling basin will be investigated. Investigating the turbulent flow field inside the stilling basin is based on the changes of two important and influential parameters, Fr and W/D .

In order to investigate the turbulent flow field, the effect of the changes in these two parameters on the longitudinal average velocity as well as the maximum velocities inside the basin, turbulent dissipation, turbulent energy

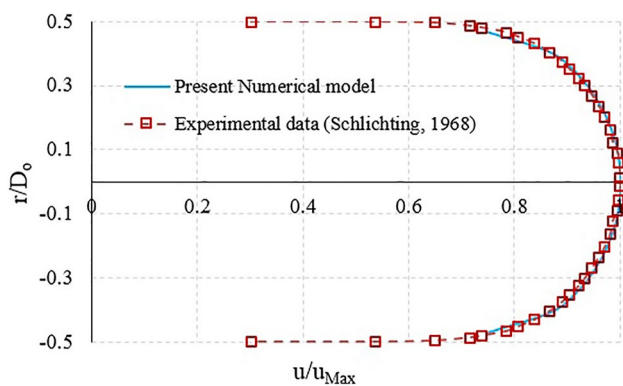


Fig. 5 Velocity profiles in the inlet pipe to the basin in the present numerical model and Schlichting laboratory result (Schlichting 1968)

Table 6 Dimensional pressure at a stagnation point on the vertical baffle

$P / \frac{\rho \bar{u}^2}{2}$ of numerical model (cm)	$P / \frac{\rho \bar{u}^2}{2}$ of physical model (cm)	Location of the recorded pressure
1.22	1.16	Stagnation point on the baffle

dissipation rate and turbulence kinetic energy have been studied. Investigating these details of the turbulent flow will lead to a better understanding of the energy dissipation mechanism inside the basin and optimal design.

Numerical model validation

In order to validate the numerical model, the results of Behnamtalab et al. (Behnamtalab et al. 2017) physical model were used. In that physical model, due to the high velocity of the flow, the complexity of the structure’s geometry, and the high turbulence of the flow, only the pressure on the middle baffle was taken using pressure transducer sensors, and there is no other data to compare with the numerical model. Therefore, to check the results and accuracy of the numerical model more precisely, the velocity profile in the inlet pipe in the present numerical model was also compared with the results of the velocity profile in the Schlichting (1968) physical model.

Figure 5 compares the longitudinal velocity profiles in the inlet pipe to the stilling basin in the present numerical model and the Schlichting (1968) laboratory results. In this figure, u is the longitudinal velocity in the inlet pipe and u_{max} is the maximum longitudinal velocity in the inlet pipe and it is observed that the result of the numerical model agrees with the laboratory model result and the average error is approximately 1.2%. Also, in Table 6, dimensionless

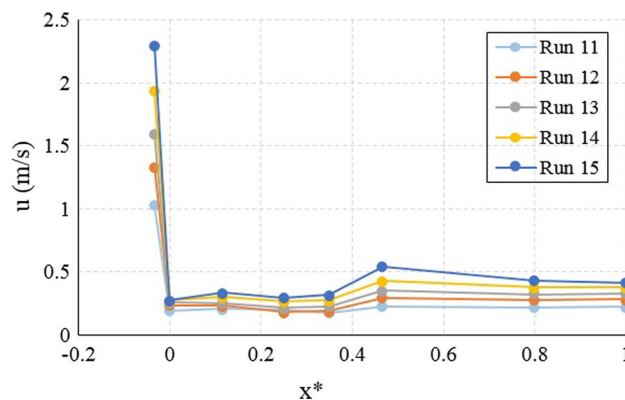


Fig. 6 Average longitudinal velocity changes along USBR VI stilling basin at $W/D = 3.50$

Table 7 Specifications of average and maximum longitudinal velocity along the USBR VI stilling basin

$W/D = 9.23$	$W/D = 5.97$	$W/D = 3.50$	
97	92	80	$\left(\frac{\bar{u} - \bar{u}_{x^*=1}}{\bar{u}} \right) \times 100$
87	68	40	$\left(\frac{u_{max,x^*=0} - u_{max,x^*=1}}{u_{max,x^*=0}} \right) \times 100$

pressure at the location of the stagnation point on the vertical baffle (the stagnation point is located along the center line of the inlet pipe on the vertical baffle) is presented in the numerical model and Behnamtalab et al. laboratory model (Behnamtalab et al. 2019). In this table, the stagnation point pressure (P) is dimensionless by the average velocity of the inlet flow to the basin (u). The result presented in the table show that the present numerical model predicts the stagnation pressure on the vertical baffle with a 5% error.

Longitudinal velocity

Figure 6 shows the changes in the average longitudinal velocity from the beginning to the end of the basin for $W/D = 3.50$ at different Fr. It can be seen that the average flow velocity has decreased sharply as soon as it enters the basin from the pipe and has an almost constant value along the basin. However, after passing the flow under the baffle (from $x^* = 0.43$ to $x^* = 1$), it increases slightly and then continues with an almost constant value to the end of the basin. The same is true for other W/D ratios. However, the average longitudinal velocity drop varies in different W/D ratios. Also, due to the fact that the cross-sectional area of the flow passing under the middle baffle is the same for different Froude numbers, so in this range, the average velocities at different Froude numbers are close to each other.

Table 7 also shows the decrease percentage in the average longitudinal velocity of the flow at the end of the basin

relative to the average longitudinal velocity of the flow in the inlet pipe. According to this table, for example, the average velocity at the end of the basin is 80% of the average velocity in the inlet pipe for every 5 Fr surveyed at $W/D=3.50$ (Run 11 to Run 15). It is observed that with increasing W/D , the decrease percentage in average longitudinal velocity relative to the average velocity of the inlet flow to the basin also increases.

Also, in this table, the reduction rate of the maximum longitudinal velocity at the end of the basin ($x^* = 1$) compared to the maximum velocity at the beginning of the basin ($x^* = 0$) is presented. The results show that in $W/D=3.50$ maximum velocity along the basin is 40%, in $W/D=5.97$ maximum velocity along the basin is 68% and in $W/D=9.23$ maximum velocity along the basin has been reduced by 87%. This result is completely consistent with the results of the study of the average velocity along the basin and confirms the fact that with increasing the W/D ratio, the average flow characteristics inside the basin will decrease more significantly.

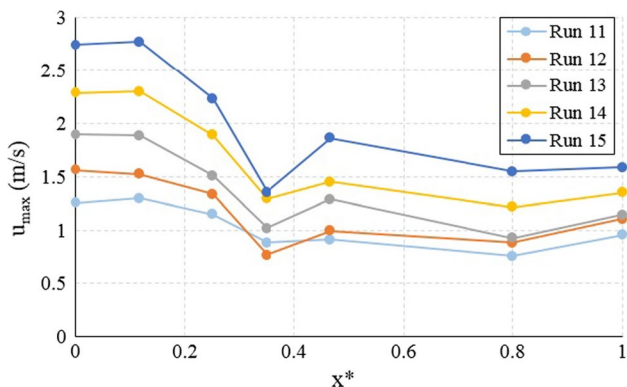


Fig. 7 maximum longitudinal velocity changes along USBR VI stilling basin at $W/D=3.50$

Fig. 8 Turbulent dissipation rate range changes in the Run 3 model

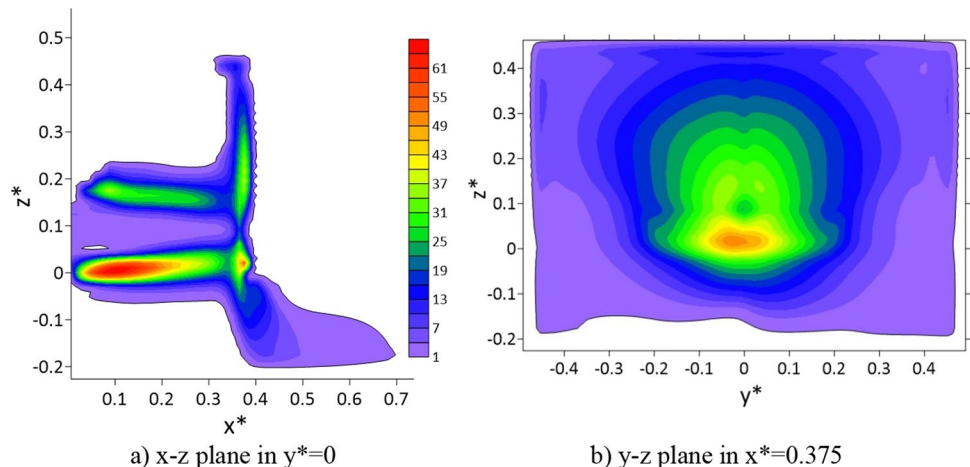


Figure 7 shows the maximum longitudinal velocity changes from the beginning to the end of the basin for $W/D=3.50$. Increasing the Froude number has increased the maximum longitudinal velocity in different parts of the basin. Also, in this table, the maximum flow velocity at the end of the basin compared to the average velocity of the inlet flow is calculated. It can be seen that in $W/D=9.23$, the maximum velocity at the end of the basin has drastically decreased compared to the average velocity at the entrance. This is very important in protecting the downstream bed of the basin. Therefore, increasing the W/D causes both the average outlet velocity and the maximum velocity to decrease more sharply at the outlet of the basin.

Turbulent dissipation

Figure 8 shows the contours of turbulent dissipation rate changes in the Run 3 model. Figure 8a shows the turbulent dissipation rate on the $x-z$ plane at $y^*=0$, and Fig. 8b shows the turbulent dissipation rate on the $y-z$ plane at $x^*=0.375$ or in other words at the upstream surface of the baffle. Incidents that occur at the boundaries of inlet jet to the basin have a maximum turbulent dissipation rate and are gradually reduced. This is due to turbulent flow fluctuations at the boundary of inlet jet to the basin. In the range of jet impact to the baffle, the turbulent dissipation rate shows higher values than remaining surface of the baffle. This is also due to changes in flow from the longitudinal direction to the vertical direction.

Figure 9 shows the turbulent dissipation rate changes at $W/D=9.23$ at different Fr . Figure 9a shows the turbulent dissipation rate changes along the basin, Fig. 9b shows the changes in the width direction of the basin and Fig. 9c shows the changes in the height direction of the basin. As shown in Fig. 9a, the maximum turbulent dissipation rate occurs near the baffle (the location of the baffle is at $x^*=0.37$). Also, the turbulent dissipation rate upstream the baffle area is higher

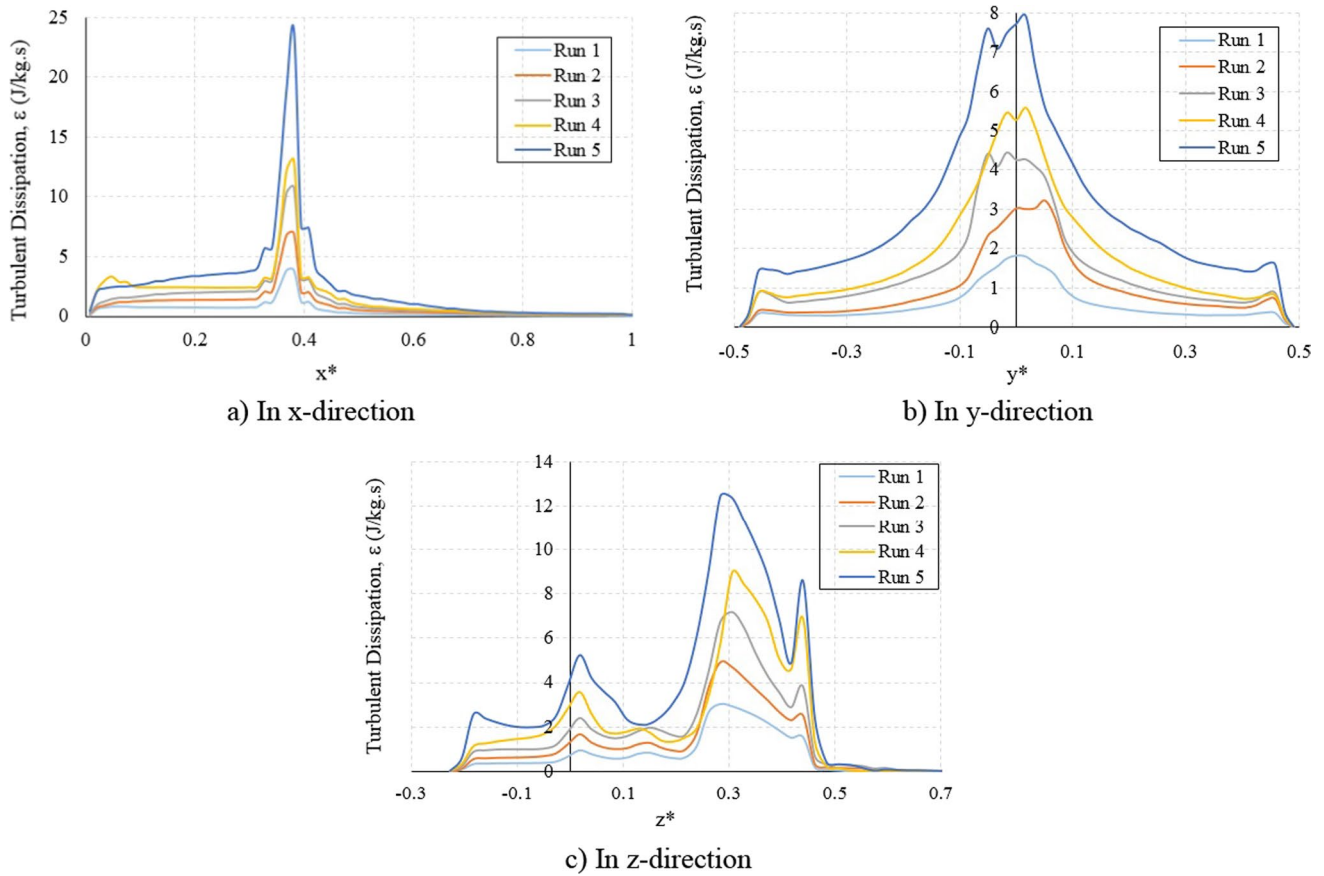


Fig. 9 Turbulent dissipation rate changes in $W/D=9.23$

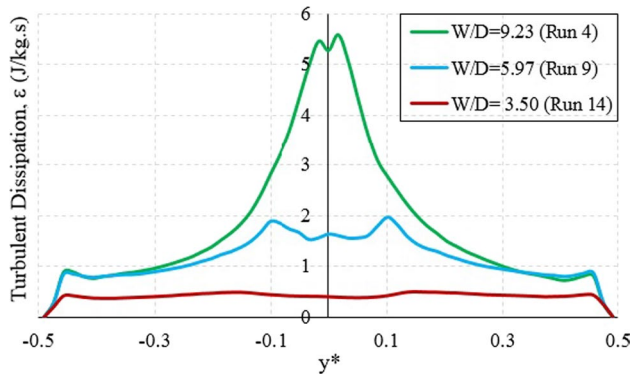


Fig. 10 Turbulent dissipation rate changes across the basin at different W/D

than the downstream area of the baffle. The turbulent dissipation rate distribution in the width direction of the basin is nonuniform and increases as it approaches the inlet pipe area ($-0.1 < y^* < 0.1$).

In Fig. 10, the turbulent dissipation rate changes across the basin for the three different W/D are compared. As

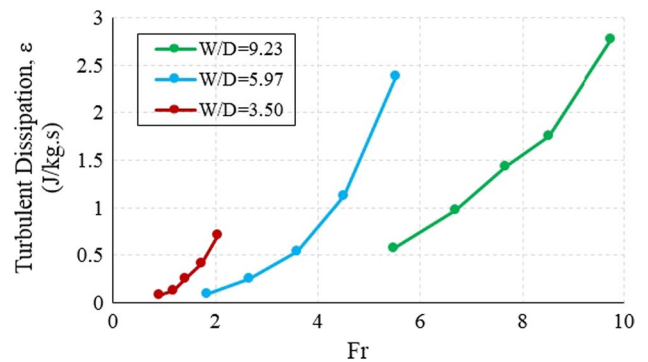


Fig. 11 Average turbulent dissipation rates at different W/D and Fr

can be seen, with increasing W/D or in other words with decreasing the inlet volume flow rate to the USBR VI stilling basin, the uniformity of the turbulent dissipation rate across the basin decreases and the maximum dissipation rate values within the inlet pipe range ($-0.1 < y^* < 0.1$) is located. As W/D decreases, the turbulent dissipation rate will have a fairly uniform distribution across the basin.

Figures 11 and 12 show the average turbulent dissipation rate. Figure 11 shows the average turbulent dissipation rate

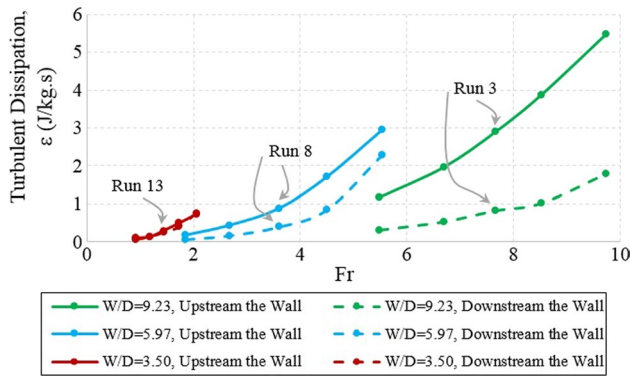


Fig. 12 Average turbulent dissipation rate upstream and downstream the baffle at different W/D and Fr

in the whole basin at different W/D ratios and Fr . Depending on the figure, the average turbulent dissipation rate in the whole basin increases with increasing W/D . Also, with increasing Fr in each W/D , the turbulent dissipation rate increases.

Figure 12 shows the average turbulent dissipation rate upstream the baffle of the basin and the average turbulence dissipation rate downstream the baffle of the basin at different W/D and Fr . It is noteworthy that with increasing W/D , the average turbulent dissipation rate at upstream of the baffle increases compared to the average turbulent dissipation rate at downstream of the baffle. At $W/D = 9.23$, the average turbulent dissipation rates are significantly different at upstream and downstream of the baffle. This indicates that increasing W/D , most of the kinetic energy of the turbulent inlet flow to the basin, in the upstream the baffle is dissipated. At $W/D = 3.50$, the average turbulent dissipation rates at upstream and downstream of the baffle are equal. The turbulent dissipation rate at upstream of the baffle for $W/D = 3.50$ (Run 13) is 0.284 j/kg s , at $W/D = 5.97$ (Run 8) at 0.881 j/kg s and at $W/D = 9.23$ (Run 1) is equal to 2.907 j/kg s . Also, the turbulent dissipation rate at downstream the baffle, for $W/D = 3.50$ (Run 13) equal to 0.249 J/kg s , at $W/D = 5.97$ (Run 8) equal to 0.394 J/kg s and in the ratio $W/D = 9.23$ (Run 1) is equal to 0.823 j/kg s . It can be seen that the turbulent dissipation rate at upstream the baffle is 14, 124 and 253% higher for $W/D = 3.50$, $W/D = 5.97$ and $W/D = 9.23$, respectively, i.e., with increasing W/D , turbulent flow energy dissipation occurs mostly at upstream the baffle, and the flow passing under the baffle will be transmitted to the downstream channel with almost constant energy.

Turbulent energy dissipation rate

Figure 13 shows the turbulent energy dissipation rate in the USBR VI stilling basin at different W/D and Fr . Turbulent energy dissipation rate is in joules per second, which is the

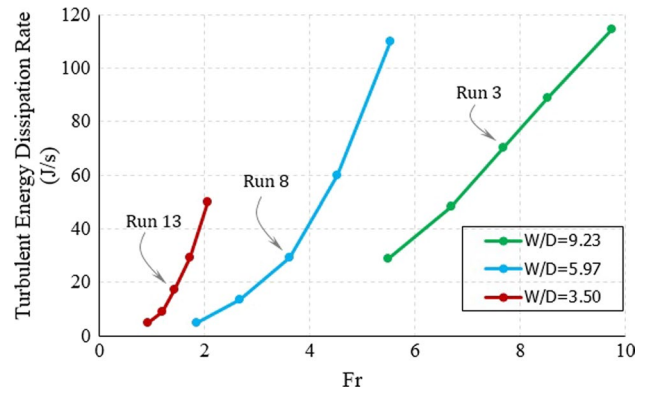


Fig. 13 Turbulent energy dissipation rate in different W/D and Fr

energy loss in the basin due to turbulent flow. The results of this diagram show that by increasing the W/D , the turbulent energy of flow is dissipated more rapidly in the basin. Also, by increasing the Froude number in each W/D , the turbulent energy dissipation rate will increase even more sharply. The remarkable result is that in the standard design performed using Eq. (3) in $W/D = 3.50$ (Run 13), the amount of the turbulent energy dissipation is equal to 17.33 j/s , in the ratio $W/D = 5.97$ (Run 8) the amount of the turbulent energy dissipation is equal to 29.30 j/s and in $W/D = 9.23$ (Run 1) the amount of the turbulent energy dissipation is equal to 70.37 j/s .

Figure 14 shows the changes in turbulent energy dissipation rate inside the basin over time in the numerical models. It observed that after the flow enters the basin through the inlet pipe and with very small fluctuations, the amount of this parameter tends to a constant value and remains constant in this value.

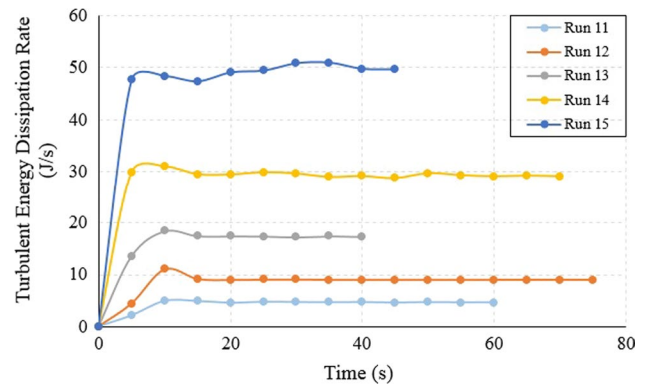


Fig. 14 Temporal changes in turbulent energy dissipation rate in $W/D = 3.50$ and different Fr

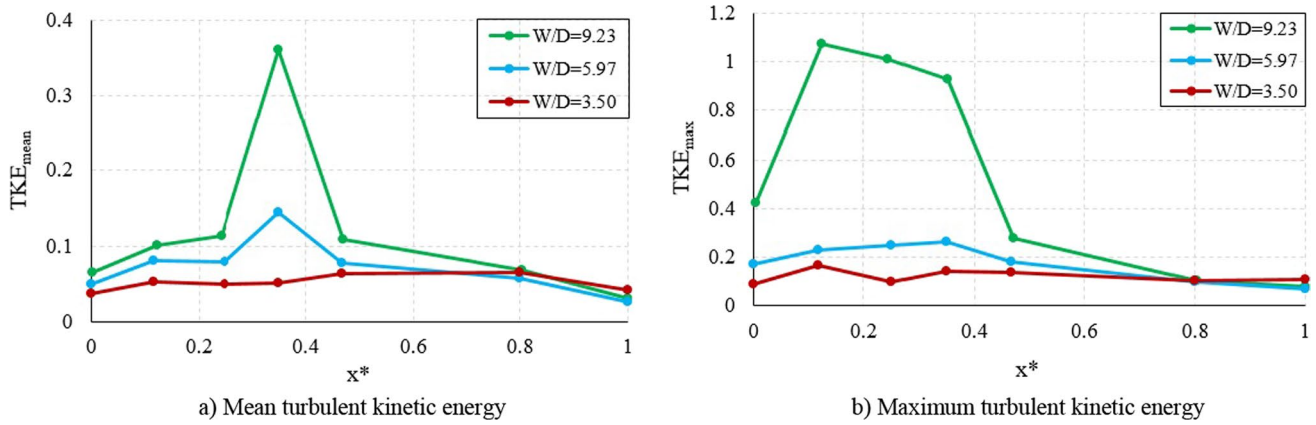


Fig. 15 Turbulent kinetic energy changes along the basin at different W/D ratios

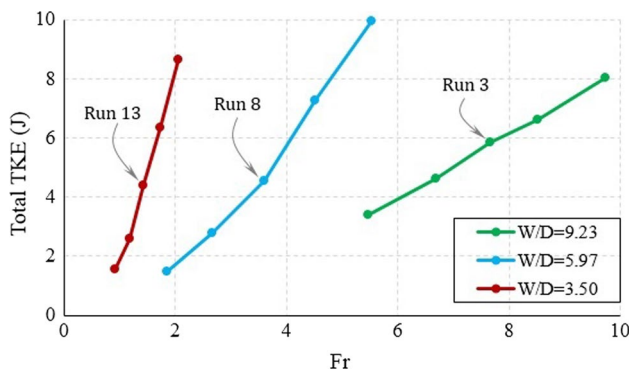


Fig. 16 Total turbulent kinetic energy inside the USBR VI stilling basin at different W/D and Fr

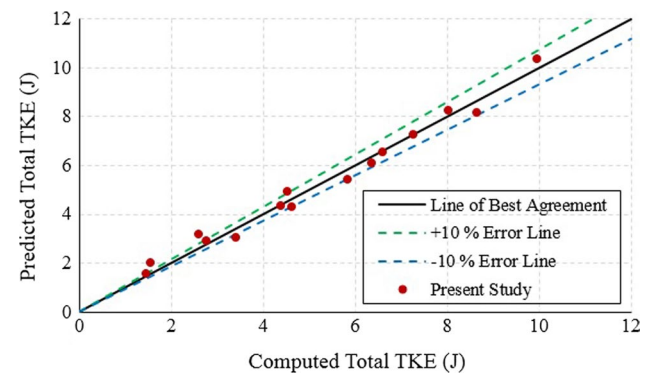


Fig. 17 Accuracy of Eq. 9 in predicting the turbulent kinetic energy inside the USBR VI stilling basin

Turbulent kinetic energy

In this section, the turbulent kinetic energy is studied. In Fig. 15 the average and maximum kinetic turbulent energy changes along the basin in different W/D ratios in the models Run 3 ($W/D = 9.23$), Run 8 ($W/D = 5.97$) and Run 13 ($W/D = 3.50$) have been compared with each other. As shown in Fig. 15a, with increasing W/D ratio, the turbulent kinetic energy at the location of flow impact with the baffle ($x^* = 0.37$) is greatly increased. As shown in Table 3, the average velocity of the flow entering the basin in Run 3, Run 8 and Run 13 models is 5.30, 3.10 and 1.60 m/s, respectively, and according to Fig. 15a the average kinetic turbulent energy at the location of flow impact with the baffle in the Run 3 model is much larger than the other two models. Due to the fact that at the point of flow impact to the baffle, especially at the stagnation point, the longitudinal velocity of the flow will reach zero, so the maximum turbulent kinetic energy occurred in the model at a higher velocity flow. Also, in Fig. 15b the maximum turbulent

kinetic energy in the Run 3 model or in other words in $W/D = 9.23$ is very different from the other two models.

In Fig. 16, the total turbulent kinetic energy changes inside the USBR VI stilling basin at different W/D ratios and Froude numbers are compared. In this diagram, the turbulent kinetic energy in the stilling basin range, i.e., $x^* = 0$ to $x^* = 1$, is calculated for Run 1 to Run 15 models. According to the standard design performed using Eq. (3) at $W/D = 3.50$ (Run 13) the amount of the total turbulent kinetic energy is 4.39 j, at $W/D = 5.97$ (Run 8) the amount of the total turbulent kinetic energy is equal to 4.54 j and in the ratio $W/D = 9.23$ (Run 3) the amount of total turbulent kinetic energy is equal to 5.83 j. This indicates that with increasing W/D ratio, the total turbulent kinetic energy inside the stilling basin is highly dependent on the W/D ratio in the standard design.

Equation 9 can be used to calculate the total turbulent kinetic energy inside the basin. In this equation, the turbulent kinetic energy inside the basin will be calculated in terms of the W/D ratio and Fr of the inflow to the basin. The accuracy

of this equation based on the prediction of available data is also presented in Fig. 17.

$$\text{Total TKE}(J) = 76.550 \times \left(\frac{W}{D}\right)^{-2.779} \times (\text{Fr}_o)^{1.733} R^2 = 0.982 \quad (9)$$

Summary and conclusions

In this research, the characteristics of Mean and turbulent flow field in USBR VI stilling basin have studied, numerically. This research has done by solving RANS equations in incompressible flow using $k - \epsilon$ RNG turbulence model. The results showed that there is a good agreement between the laboratory data and the results of the present numerical model using mesh cell size and sensitivity analysis of turbulence models. The general results of this research are as follows:

- The mean and maximum longitudinal velocity at $W/D = 3.50$ ratio along the basin were 80 and 40%, respectively, at $W/D = 5.97$ ratio at 92 and 68%, respectively, and at $W/D = 9.23$ ratio at 97% and It is reduced by 87%.
- By increasing the W/D ratio, the average velocity and the maximum velocity at the end of the basin will decrease more sharply.
- The turbulence dissipation rate in the upstream of the baffle is higher than the downstream of the baffle.
- The distribution of turbulent dissipation rate across the basin is nonuniform and increases as it approaches the inlet pipe area ($-0.1 < y^* < 0.1$).
- As W/D increases, the uniformity of the turbulent dissipation rate across the basin decreases.
- The average turbulent dissipation rate in the whole basin increases with increasing W/D ratio. Also, with increasing the Froude numbers in each W/D ratio, the turbulent dissipation rate increases.
- By increasing the W/D ratio, the average turbulent dissipation rate at upstream of the baffle increases compared to the average turbulent dissipation rate at downstream of the baffle.
- the turbulent dissipation rate at upstream of the baffle than the downstream of the baffle is 14, 124 and 253% higher for $W/D = 3.50$, $W/D = 5.97$ and $W/D = 9.23$, respectively, i.e., with increasing W/D , the turbulent flow energy dissipation occurs mostly at upstream of the baffle.
- As the W/D increases, the turbulent flow energy is dissipated more rapidly into the basin.
- By increasing the W/D , the total turbulent kinetic energy inside the stilling basin is highly dependent on the W/D in the standard design.
- In this research, based on the analysis of the mean and turbulent flow field in the USBR VI stilling basin, it is proposed to increase the W/D as much as possible in the design of these basins, based on the existing real conditions.

Funding The Authors received no specific funding for this work.

Declarations

Conflict of Interest On behalf of all authors, the corresponding author states that there is no conflict of interest.

Open Access This article is licensed under a Creative Commons Attribution 4.0 International License, which permits use, sharing, adaptation, distribution and reproduction in any medium or format, as long as you give appropriate credit to the original author(s) and the source, provide a link to the Creative Commons licence, and indicate if changes were made. The images or other third party material in this article are included in the article's Creative Commons licence, unless indicated otherwise in a credit line to the material. If material is not included in the article's Creative Commons licence and your intended use is not permitted by statutory regulation or exceeds the permitted use, you will need to obtain permission directly from the copyright holder. To view a copy of this licence, visit <http://creativecommons.org/licenses/by/4.0/>.

References

- Aleyasin SS, Fathi N, Vorobieff P (2015) Experimental study of the Type VI stilling basin performance. *J Fluids Eng* 137(3):034503
- Amorim BJCC, Amante RCR, Barbosa VD (2015) Experimental and numerical modeling of flow in a stilling basin. In: 36th IAHR World Congress, Hague, the Netherlands.
- Anderson J, Wendt J (1995) *Computational fluid dynamics*, vol 206. McGraw-Hill, New York.
- Babaali H, Shamsai A, Vosoughifar H (2015) Computational modeling of the hydraulic jump in the stilling basin with convergence walls using CFD codes. *Arab J Sci Eng* 40(2):381–395
- Baranya S, Olsen NRB, Józsa J (2015) Flow analysis of a river confluence with field measurements and RANS model with nested grid approach. *River Res Appl* 31(1):28–41
- Barati R, Neyshabouri SAAS, Ahmadi G (2018) Issues in Eulerian–Lagrangian modeling of sediment transport under saltation regime. *Int J Sediment Res* 33(4):441–461
- Behnamtalab E, Ghodsian M, Zarrati AR, Salehi Neyshabouri SAA (2017) Numerical simulation of Flow Field in Stilling Basin USBR VI. *Iran J Irrigat Drain* 11(5):822–838 (in Persian)
- Behnamtalab E, Ghodsian M, Zarrati AR, Salehi Neyshabouri SAA (2019) Geometry modification of stilling basin USBR VI with numerical simulation. *J Hydraul Iran Hydraul Assoc*, pp 1–15 (in Persian).
- Behnamtalab E, Lakzian E, Hosseini SB (2022) Study of USBR VI Stilling Basin with Entropy Generation Index. *Exp Techniques*, pp 1–16.

- Beichley GL (1971) Hydraulic design of stilling basin for pipe or channel outlets. A Water Resources Technical Publication, Research Report No. 24, United States Department of the Interior, Bureau of Reclamation, Division of Research, Denver, Colorado
- Bestawy A, Hazar H, Ozturk U, Roy T (2013) New shapes of baffle piers used in stilling basins as energy dissipators. *Asian Trans Eng (ATE)* 3(1):1–7
- Blaisdell F (1992) Discussion of “HGL elevation at pipe exit of USBR Type VI impact basin” by Charles E. Rice and Kem C. Kadavy (1991, 117, 7). *J Hydraul Eng-Asce* 118(7):1076–1077.
- Brevard JA (1971) Criteria for the hydraulic design of impact basins associated with full flow in pipe conduits. Technical release (United States. Soil Conservation Service); no. 49.
- Fadafan MA, Kermani MRH (2017) Moving particle semi-implicit method with improved pressures stability properties. *J Hydroinform*, jh2017121.
- Farhadi A, Mayrhofer A, Tritthart M, Glas M, Habersack H (2018) Accuracy and comparison of standard $k-\omega$ with two variants of $k-\omega$ turbulence models in fluvial applications. *Eng Appl Comput Fluid Mech* 12(1):216–235
- Ghazizadeh F, Moghaddam MA (2016) An experimental and numerical comparison of flow hydraulic parameters in circular crested weir using flow3D. *Civil Eng J* 2(1):23–37
- Goel A (2008) Design of stilling basin for circular pipe outlet. *Can J Civ Eng* 35(12):1365–1374
- Hager Willi H (2013) Energy dissipators and hydraulic jump, vol 8. Springer, Cham.
- Hirt CW (2011) CFD-101: the basics of computational fluid dynamics modeling. FLOW-3D manual. Flow Science Press, Flow Science Inc, USA
- Hirt CW, Nichols BD (1981) Volume of fluid (VOF) method for the dynamics of free boundaries. *JCP* 39:201
- Hirt CW, Sicilian JM (1985) A porosity technique for the definition of obstacles in rectangular cell meshes. In: Fourth International Conference Ship Hydrodynamics, Washington, DC, September 1985.
- Hoffman J, Claes J (2007) Computational turbulent incompressible flow: Applied mathematics: Body and soul 4, vol. 4. Springer, Cham.
- Jafari-Nodoushan E, Hosseini K, Shakibaenia A, Mousavi SF (2016) Meshless particle modelling of free surface flow over spillways. *J Hydroinform* 18(2):354–370
- Khan LA (2011) Computational fluid dynamics modeling of emergency overflows through an energy dissipation structure of a water treatment plant. In: World environmental and water resources congress 2011: Bearing Knowledge for Sustainability, pp. 1484–1493.
- Pagliara S, Palermo M (2012) Effect of stilling basin geometry on the dissipative process in the presence of block ramps. *J Irrigat Drain Eng* 138(11):1027–1031
- Peterka AJ (1978) Hydraulic design of stilling basins and energy dissipators. No. 25. Department of the Interior, Bureau of Reclamation.
- Rady RMAE (2011) 2D–3D modeling of flow over sharp-crested weirs. *J Appl Sci Res* 7(12):2495–2505
- Rice CE, Kem CK (1991) HGL elevation at pipe exit of USBR type VI impact basin. *J Hydraul Eng* 117(7):929–933
- Rodriguez JF, Bombardelli FA, García MH, Frothingham KM, Rhoads BL, Abad JD (2004) High-resolution numerical simulation of flow through a highly sinuous river reach. *Water Resour Manage* 18(3):177–199
- Schlichting H (1968) Boundary-layer theory. 6th Edn, McGraw-Hill, New York
- Flow Science, Incorporated (2008) FLOW-3D User’s Manual Version 9.3. Santa Fe, New Mexico
- Shahheydari H, Nodoushan EJ, Barati R, Moghadam MA (2015) Discharge coefficient and energy dissipation over stepped spillway under skimming flow regime. *KSCE J Civ Eng* 19(4):1174–1182
- Tajnesaie M, Jafari Nodoushan E, Barati R, Azhdary Moghadam M (2018) Performance comparison of four turbulence models for modeling of secondary flow cells in simple trapezoidal channels. *ISH J Hydraul Eng*, pp 1–11.
- Talebpour M, Liu X (2018) Numerical investigation on the suitability of a fourth-order nonlinear $k-\omega$ model for secondary current of second type in open-channels. *J Hydraul Res*, pp 1–12.
- Tiwari HL, Goel A, Sharma AK, Balvanshi A (2022) Performance improvement of Usbr VI stilling basin model for pipe outlet. In: Hydrological modeling. Springer, Cham, pp 1–8.
- Tiwari HL, Goel A (2016) Effect of impact wall on energy dissipation in stilling basin. *KSCE J Civ Eng* 20(1):463–467
- Tullis BP, Bradshaw RD (2015) Impact dissipators. *Energy Dissipation Hydraul Struct*, pp 141–168.
- Usta E (2014) Numerical investigation of hydraulic characteristics of Laleli Dam spillway and comparison with physical model study. Master’s thesis.
- Verma DVS, Goel A (2000) Stilling basins for pipe outlets using wedge-shaped splitter block. *J Irrigat Drain Eng* 126(3):179–184
- Verma DVS, Goel A (2003) Development of efficient stilling basins for pipe outlets. *J Irrigat Drain Eng* 129(3):194–200
- Vischer DL (2018) Types of energy dissipators. In: Energy dissipators. Routledge, England, pp. 9–21.
- White F (2006) Viscous fluid flow, vol 3. McGraw-Hill, New York.
- Young RB (1978) Energy dissipators: Baffled outlets. In: Aisenbrey AJ Jr (ed) Design of small canal structures. USBR, Denver, pp. 308–322
- Zachoval Z, Roušar L (2015) Flow structure in front of the broad-crested weir. In: EPJ Web of conferences, vol. 92. EDP Sciences, France, p. 02117.

Publisher’s Note Springer Nature remains neutral with regard to jurisdictional claims in published maps and institutional affiliations.